

UC Davis

UC Davis Previously Published Works

Title

Contemporary and Emerging MRI Strategies for Assessing Kidney Allograft Complications: Arterial Stenosis and Parenchymal Injury, From the AJR Special Series on Imaging of Fibrosis.

Permalink

<https://escholarship.org/uc/item/5hc2c68g>

Journal

American Journal of Roentgenology, 222(3)

Authors

Bane, Octavia

Lewis, Sara

Lim, Ruth

et al.

Publication Date

2024-03-01

DOI

10.2214/AJR.23.29418

Peer reviewed



Published in final edited form as:

AJR Am J Roentgenol. 2024 March ; 222(3): e2329418. doi:10.2214/AJR.23.29418.

Contemporary and Emerging MRI Strategies for Assessing Kidney Allograft Complications: Arterial Stenosis and Parenchymal Injury, From the *AJR* Special Series on Imaging of Fibrosis

Octavia Bane, PhD¹, Sara C. Lewis, MD¹, Ruth Lim, MD², Benjamin W. Carney, MD, MS³, Amar Shah, MD⁴, Ghaneh Fananapazir, MD³

¹Department of Radiology, Icahn School of Medicine at Mount Sinai, New York, NY.

²Department of Radiology, University of Melbourne, Austin Health, Melbourne, Australia.

³Department of Radiology, University of California Davis Medical Center, 4860 Y St, Ste 3100, Sacramento, CA 95816.

⁴Department of Radiology, Mayo Clinic Arizona, Phoenix, AZ.

Abstract

MRI plays an important role in the evaluation of kidney allografts for vascular complications as well as parenchymal insults. Transplant renal artery stenosis, the most common vascular complication of kidney transplant, can be evaluated by MRA using gadolinium and nongadolinium contrast agents as well as by unenhanced MRA techniques. Parenchymal injury occurs through a variety of pathways, including graft rejection, acute tubular injury, BK polyomavirus infection, [AQ1] drug-induced interstitial nephritis, and pyelonephritis. Investigational MRI techniques have sought to differentiate among these causes of dysfunction as well as to assess the degree of interstitial fibrosis or tubular atrophy (IFTA)—the common end pathway for all of these processes—which is currently evaluated by invasively obtained core biopsies. Some of these MRI sequences have shown promise in not only assessing the cause of parenchymal injury but also assessing IFTA noninvasively. This review describes current clinically used MRI techniques and previews promising investigational MRI techniques for assessing complications of kidney grafts.

Keywords

allograft; kidney; MRI; transplant

In patients with end-stage kidney disease, renal transplant provides greater survival benefits when compared with long-term dialysis. Given the importance of kidney grafts as well as the gap between donors and recipients, increasing graft survival is an important

Address correspondence to G. Fananapazir (fananapazir@ucdavis.edu, @ghanehf).

The authors declare that there are no disclosures relevant to the subject matter of this article.

Provenance and review: Solicited; externally peer reviewed.

Peer reviewers: Francesco Alessandrino, University of Miami; additional individual(s) who chose not to disclose their identity.

goal. Graft survival has improved over time, with 5-year survival rates steadily climbing to approximately 72% from deceased donors and 85% from living donors [1]. This improvement is attributed to many factors, including improved immunosuppression, a decline in rejection episodes, and improved matching of donors to recipients. Despite this improvement, chronic allograft injury characterized histologically by interstitial fibrosis or tubular atrophy (IFTA) remains the major cause of kidney disease progression and allograft failure [2] and is the most important predictor of outcome [3].

Imaging plays a major role in assessing kidney grafts, with the aim of improving long-term outcomes. The most common vascular complication affecting kidney grafts is transplant renal artery stenosis (TRAS) [4]. TRAS, if unrecognized and untreated, can lead to poorer graft outcomes owing to ischemia and eventual fibrosis [5]. Patients with TRAS can present with nonspecific clinical symptoms. Ultrasound serves as the primary initial imaging modality for TRAS. Doppler ultrasound techniques rely on indirect evaluation, based on flow dynamics, to indicate the presence or absence of TRAS [6, 7]. However, false-positive and false-negative results of ultrasound examinations can lead to unneeded invasive angiographic examinations or delayed recognition of TRAS. MRA can play a useful adjunct role as a noninvasive technique for patients with equivocal findings or whose clinical picture may warrant additional assessment of the vasculature despite a reassuring ultrasound appearance. Various MRA techniques are used, including gadolinium-enhanced MRA, ferumoxytol-enhanced MRA, and unenhanced sequences, all of which are used to assess for TRAS in practice. A meta-analysis that included these three techniques showed pooled sensitivity of 0.96 (95% CI, 0.76–0.99) and pooled specificity of 0.93 (95% CI, 0.86–0.96) for the detection of TRAS [8].

Incremental and cumulative allograft damage occurs from various immunologic and nonimmunologic causes, including graft rejection, acute tubular injury, BK polyomavirus infection, drug-induced interstitial nephritis, and pyelonephritis, and are often diagnosed on the basis of a combination of clinical, laboratory, and core biopsy samples. The common endpoint of these pathologic processes is the development of IFTA, which is currently assessed by a reference standard of core biopsy using the Banff classification [9]. Renal allograft fibrosis ultimately drives chronic kidney disease (CKD) progression, predicts allograft failure, and is associated with increased patient mortality [10–12]. Although complications after kidney transplant biopsies are infrequent, repeated biopsies are suboptimal for monitoring patients during trials of new therapies aimed at improving allograft survival [13].

Functional MRI methods that hold promise in evaluating the cause of allograft dysfunction or in assessing the degree of IFTA include DWI-based methods (intravoxel incoherent motion [IVIM] and diffusion-tensor imaging [DTI]), T1 mapping, T1 ρ , blood oxygenation level-dependent (BOLD) imaging, arterial spin-labeling (ASL), and phase-contrast (PC) sequences (Fig. 1). These MRI techniques are feasible in renal allografts and may provide complementary information regarding renal parenchymal tissue structure, including presence of fibrosis, evidence of rejection, and prediction of decline in allograft function and graft loss. Validation of functional MRI methods as markers of renal allograft parenchymal dysfunction would be of major clinical significance for early detection,

assessment of efficacy of novel therapeutic agents, and longitudinal disease monitoring. Although the functional methods were historically evaluated in isolation, the sequences are increasingly evaluated in combination for characterization of allograft dysfunction. Efforts to standardize protocols for the sequences underlying quantitative biomarkers of renal parenchymal disease are underway through interdisciplinary initiatives (renalMRI.org, International Society for Magnetic Resonance in Medicine [ISMRM] Renal MRI Study Group, U.S. National Institute of Diabetes and Digestive and Kidney Diseases [NIDDK], U.K. Renal Imaging Network [UKRIN]), educational activities, and large clinical studies. For example, renalMRI.org, a continuation of the European Union Magnetic Resonance Imaging Biomarkers for Chronic Kidney Disease (PARENCHIMA) collaboration, has promoted standardization of functional MRI markers in CKD through a series of consensus technical review articles [14–19]; these articles provide sample MRI protocols and guidelines for using quantitative MRI techniques in native and transplant kidneys.

Vascular Evaluation of Renal Transplants

Gadolinium-Enhanced MRA

Gadolinium-enhanced MRA became widely used after concerns were raised about a possible link between iodine-based contrast agents and kidney injury [20]. Early studies showed gadolinium-enhanced MRA to have good sensitivity for the detection of TRAS [21, 22]. However, in the early 2000s, the link was established between nephrogenic systemic fibrosis (NSF) and the use of gadolinium-based contrast agents in patients with impaired renal function [23]. Although NSF is now much less of a concern, particularly with the use of macrocyclic gadolinium agents, alternative contrast agents and unenhanced techniques continue to play roles, especially given more recent concerns about gadolinium deposition [24, 25].

Studies estimate that gadolinium-enhanced MRA has sensitivity of 59–100% and specificity of 75–100% for TRAS measuring greater than 50% [26, 27]. In a study comparing MRA and CTA to digital subtraction angiography (DSA), gadolinium-enhanced MRA performed at a level similar to CTA, providing a nonionizing and nonnephrotoxic alternative [27].

Gadolinium-enhanced MRA can be limited by susceptibility artifact from vascular or surgical clips at the anastomosis, with one study showing such artifact in two of 13 patients [27]. In our experience, this artifact is rarely limiting.

Ferumoxytol-Enhanced MRA

Ferumoxytol is an ultrasmall superparamagnetic iron oxide (USPIO) nanoparticle that was first developed as an injectable MRI contrast agent. Its manufacturers, however, obtained FDA approval for its therapeutic use as treatment of iron-deficiency anemia in patients with renal failure [28]. Nevertheless, its imaging characteristics as a blood pool agent, along with its prolonged intravascular half-life of 14 hours, make ferumoxytol an appealing alternative to gadolinium-based contrast agents for vascular evaluation [28]. This long half-life allows repeat imaging of the vasculature potentially days after a single injection. The long half-life also permits longer pulse sequences, which may provide increased resolution

of small vessels, including the ability to depict vessels approaching 1 mm in diameter [29] (Fig. 2). Additionally, the lack of significant parenchymal enhancement results in the ability to carefully assess intraparenchymal vessels, which may be poorly assessed on gadolinium-enhanced MRA owing to parenchymal uptake [30]. Acquisition times can be shorter for ferumoxytol-enhanced MRA compared with unenhanced MRA, potentially decreasing motion artifact [30].

Ferumoxytol-enhanced MRA has good performance using DSA as the reference standard and, unlike some unenhanced MRA sequences, can depict stenosis even in branches of the renal arteries and in the setting of tortuous vascularity [31]. One study evaluated the accuracy of ferumoxytol-enhanced MRA in 42 stenoses [31]. In that study, the sensitivity and specificity for substantial stenoses was 100% and 75–87.5%, respectively [31]. This diagnostic performance compares favorably with the results of a pooled assessment of six studies evaluating gadolinium-enhanced MRA [8]. However, direct comparison between ferumoxytol-enhanced MRA and gadolinium-enhanced MRA has not been performed to our knowledge. Similar to other MRA methods, ferumoxytol-enhanced MRA may slightly overestimate degrees of stenosis compared with DSA [31].

Although ferumoxytol is the most widely used non-gadolinium-based MRI agent for renal transplant evaluation, its use remains limited by potential lack of drug availability and incomplete clinical adoption. Although currently in phase 3 trials, a second USPIO, ferumoxtran-10, shows similar imaging findings as ferumoxytol but has a longer half-life (24–36 hours) and possibly has a better safety profile [32].

Unenhanced MRA

Unenhanced MRA removes concerns regarding exogenous contrast media and need for IV access. Inflow inversion recovery (IFIR) is an easily implemented MRI technique with wide commercial availability that has been used to evaluate renal graft arteries. An axial volume is typically prescribed with a balanced SSFP (bSSFP) readout, fat suppression, and a slab-selective radiofrequency inversion pulse to suppress background signal [33]. Longer inversion time (TI) improves inflow of arterial spins at the expense of recovery of background signal, with typical TI of 1200 ms at 1.5 T. Imaging at 3 T enables longer TI owing to longer T1 relaxation times of background tissue and therefore greater arterial inflow. ECG-gating [33–36] or a respiratory navigator can improve image quality at the expense of efficiency.

IFIR has high sensitivity for TRAS (Fig. 3). Zhang et al. [37] showed a sensitivity of 100% in 330 patients and an accuracy of 96.6% in a subset of 22 patients with DSA correlation. Lanzman et al. [36] reported sensitivity of 100% and specificity of 88% for TRAS with ECG-gating ($n = 20$). Smaller studies also reported unenhanced MRA to have good correlation with contrast-enhanced MRA [38] and DSA [39].

A challenge with IFIR is inadequate arterial inflow in patients with low-flow states [36, 37]. Susceptibility artifact from surgical clips can obscure target vasculature owing to bSSFP readout [36]. As with all flow-dependent techniques, dephasing from turbulent flow can cause overestimation of stenosis [36, 39]. Spatial resolution limitations and motion artifact

from breathing or peristalsis may impact visualization of small or accessory arteries and hinder image quality [37]. Strategies to improve IFIR image quality include the following: for low output states, increasing TI to maximize arterial inflow, although contrast to background tissue will be reduced; for susceptibility artifact, applying shim targeted only to the area of interest, imaging at lower field strength (i.e., 1.5 T instead of 3 T), minimizing TE and TR, and increasing receiver bandwidth at the expense of SNR; for motion artifact, training patients to maintain shallow breathing, and targeting the volume to cover only the vessels of interest and to minimize imaging time [40].

There is limited experience and commercial availability for alternative approaches to IFIR. Serhal et al. [41] evaluated quiescent-interval slice-selective (QISS) MRA, a 2D flow-dependent ECG-gated bSSFP technique developed for peripheral arterial assessment. QISS MRA provided diagnostic image quality in 100% of 43 patients with suspected TRAS, compared with 86% for IFIR, and both techniques showed high accuracy for stenosis compared with DSA.

Parenchymal Evaluation

DWI

DWI is based on microscopic motion of water molecules in biologic tissues and is determined by tissue cellularity, the size of the extracellular extravascular space, and the presence of macromolecules (i.e., collagen in the setting of fibrosis). ADC is a quantitative measure derived from monoexponential decay of a tissue's MR signal intensity. ADC integrates cellular diffusion and capillary perfusion into one parameter [42]. Studies have established an association or negative correlation between cortical ADC or corticomedullary difference in ADC values and interstitial fibrosis for murine models [43, 44] and human transplant kidneys [45–48]. In human renal allografts, moderate negative correlation was reported between cortical ADC and interstitial fibrosis assessed by Masson trichrome stain, and corticomedullary difference in ADC values correlated with estimated glomerular filtration rate (eGFR) and interstitial fibrosis [46, 48, 49]. The inverse correlation of ADC with interstitial fibrosis was significant in a study of 103 allografts with acute dysfunction undergoing biopsy, supporting the concept that DWI with ADC is useful for predicting IFTA irrespective of concomitant diagnoses [48]. Inflammation severity and edema were also assessed after kidney transplant in mice. ADC showed progressive reduction in allogeneic grafts compared with isogenic grafts and normal kidneys, paralleling histologic cellular infiltration and tissue inflammation [50]. Cortical ADC also predicts rate of annual decline in eGFR [51]. These studies indicate that a decrease in cortical ADC is a useful marker of fibrosis (Fig. 1) but can be confounded by other changes in renal parenchyma arising from inflammation or infection.

Intravoxel Incoherent Motion DWI

Microperfusion also contributes to DWI signal decay. IVIM-DWI [52] is an advanced DWI technique (Fig. 4) that separates contributions of microvascular perfusion (D^*) and perfusion fraction (PF; the fraction of the voxel that is occupied by vessels) from true intracellular water diffusion (D). Significant correlations were found between cortical D^* and Banff

interstitial fibrosis scores and between PF and Banff chronic inflammation [48, 53]. IVIM-DWI has shown value over standard ADC by showing significantly reduced PF in allografts with acute rejection, with no significant differences in ADC between stable function and rejection; these findings were found to represent reductions in microcirculation rather than in pure cellular diffusion [54]. Significant correlations in multiparametric MRI were found for dysfunctional allografts and histopathologic parameters reflecting glomerular and vascular dysfunction and inflammation. Cortical PF on IVIM-DWI negatively correlated with Banff scores for glomerulosclerosis, vascular intimal thickening, and peritubular capillaritis (Fig. 4). Cortical ADC was negatively correlated with peritubular capillaritis and glomerulitis scores, whereas D was negatively associated with the glomerulitis score. Cortical ADC had excellent diagnostic performance in distinguishing no or mild from moderate or severe combined glomerulitis with peritubular capillaritis [55].

In addition to cortical ADC and medullary ADC, D on IVIM-DWI was significantly decreased in fibrotic allografts compared with allografts with stable function [55] (Fig. 1). A separate study in 47 patients compared ADC to IVIM parameters for assessment of IFTA, acute changes (acute interstitial inflammation, peritubular capillaritis, glomerulitis, and tubulitis), and chronic changes (IFTA, vascular intimal thickening, and chronic glomerulopathy) [56]; cortical PF was superior to ADC for identifying both mild and severe acute changes, although ADC was equivalent to or better than D or PF alone for evaluating chronic changes. The findings support the complementary nature of ADC derived from monoexponential analysis and parameters derived from biexponential analysis in increasing diagnostic performance for discriminating the severity of pathologic changes in the allograft. Finally, cortical ADC and D* predict graft loss or relisting independent of clinical and demographic characteristics, and medullary ADC predicts graft loss or relisting independent of clinical or demographic and histopathologic characteristics [55].

Diffusion-Tensor Imaging

DTI can be used to probe tissue microstructure by determining the preferred diffusion direction, reflected in the fractional anisotropy (FA) (Fig. 4) parameter, in addition to calculating the global diffusion (mean diffusivity [D_{mean}] or mean ADC) [57]. FA is a scalar value between 0 and 1, with a value of 0 indicating isotropic diffusion (i.e., unrestricted or equally restricted in all directions) and a value of 1 indicating anisotropic diffusion (i.e., along one dominant or preferred direction). Studies have confirmed that renal medullary FA is higher than cortical FA, owing to renal pyramid architecture [57–60]. Medullary FA decreases with renal dysfunction and is positively correlated with eGFR in transplanted kidneys [57, 59, 60]. DTI tractography displays dominant diffusion directions and shows reduced diffusion tract density in patients with impaired renal function [57, 58, 60]. Reduction of FA and of tract density is potentially caused by tubular atrophy, interstitial fibrosis, cellular infiltration, and scarring of tubuli, although published results are mixed [57, 58, 60]. In a prospective study of 20 patients with unconfounded renal allograft rejection and 22 patients with stable allograft function, cortical and medullary FA values showed AUCs of 0.853 and 0.757, respectively, for differentiating rejection from stable function, whereas cortical and medullary ADC measurements showed AUCs of 0.709 and 0.736, respectively [61]. A prospective study showed positive correlation of cortical DTI FA with inflammation

in the area of the IFTA, which the authors referred to as the i-IFTA score [55], contrary to observations of reduced anisotropy with IFTA and cellular infiltration in a separate study [45].

Limitations of DWI include sensitivity to motion and signal biases introduced by gradient nonlinearity in organs away from isocenter, such as renal allografts, and by shim and eddy currents. Motion artifacts are a lesser issue with renal allografts than with native kidneys, and newer technical developments have enabled motion correction through respiratory gating and b-value image coregistration integrated into DWI reconstruction on the scanner. Bias introduced by gradient nonlinearity for multiplatform studies can be assessed using an ice-water DWI phantom [62].

T1 Mapping

T1 mapping maps each pixel to the tissue's T1 spin-lattice relaxation time (Fig. 5). T1 relaxation measurements depend on both the molecular environment of water molecules and the pathologic changes in tissue. T1 correlates with tissue fibrosis owing to association with collagen as well as with inflammation from cellular swelling and interstitial edema. In a study of animal and human renal allografts, both T1 and ADC were associated with IFTA. Corticomedullary differences in T1 (T1) and ADC (ADC) predicted interstitial fibrosis by Masson trichrome stain and Sirius red stain but not inflammation [46]. The combination of T1 and ADC showed improved performance for fibrosis detection compared with the variables alone, suggesting that the two values measure slightly different processes [49]. In a murine model of ischemia- and reperfusion-induced acute kidney injury, T1 values were associated with early inflammation (day 7), and increased T1 values were observed through day 28 in more severe acute kidney injury [63]. Human studies have confirmed significant associations for T1 values and moderate or severe interstitial fibrosis and total inflammation [47]. These results agree with a study of 16 patients with biopsy correlation in which cortical T1 values distinguished moderate or severe IFTA from no or mild IFTA [55]. That study found excellent performance of T1 for IFTA; this performance was improved by combination with cortical ADC in a binary logistic model [55]. Leave-one-out cross-validation of the regression model combining T1 and cortical ADC confirmed high diagnostic performance [55]. This study also found that cortical T1 measurement predicted graft loss or relisting independent of clinical and demographic characteristics [55].

Currently, the reference standard for measurement is manual ROI analysis, which is time-consuming and requires observer training. Excellent test-retest and interobserver repeatability in the cortex and medulla have been shown for T1 measurement as well as for D on IVIM-DWI and ADC [55]. A study investigated the role of automated corticomedullary T1 measurement for assessment of renal function (eGFR) and fibrosis using a deep learning-based 2D U-Net (XXX [RCM] U-Net) to autosegment renal cortex and medulla of the renal allograft T1 maps and autocalculate T1 values. In agreement with prior studies, T1 values were lower in patients with cellular rejection compared with T1 values in both patients without rejection and those with humoral rejection [64]. For eGFR and fibrosis assessment, the RCM U-Net correlation coefficient and R^2 values showed better correlation with eGFR and renal percentage fibrosis than did manual ROI

values [64]. Furthermore, RCM U-Net showed 50% less mean absolute error, 16% better Dice coefficient score, and 12% improved results in terms of sensitivity over conventional convolutional neural networks [64].

T1 ρ

T1 ρ is an emerging biomarker (Fig. 5) for noninvasive assessment of fibrosis in the liver [65, 66]; myocardium [67, 68]; and, more recently, renal allografts [69]. Decay of transverse magnetization in the presence of a spin-lock radiofrequency field is determined by the spin-lattice relaxation time constant in the rotating frame, termed “T1 ρ ,” and provides tissue contrast [66]. T1 ρ is sensitive to interactions between water molecules and collagen [70]. An animal study showed that increase in liver T1 ρ values is driven mostly by fibrosis and not by inflammation [71]. A paucity of literature has investigated T1 ρ in the kidney. An initial study showed differences in T1 ρ measurement in patients with lupus nephritis compared with healthy control patients [68]. In a prospective pilot study in functional and fibrotic allografts, AUC of T1 ρ for differentiating functional allografts from chronic dysfunction with fibrosis was 0.77, with sensitivity of 75.0% and specificity of 86.7% [69]. T1 ρ may thus provide an indirect measurement of collagen deposition due to renal allograft IFTA.

Blood Oxygenation Level–Dependent MRI

BOLD MRI relies on the paramagnetic properties of deoxygenated hemoglobin, which increases the transverse relaxation rate (R2*) (Fig. 5) of water protons and decreases multiecho gradient-recalled echo MRI signal. The method has received considerable interest for assessing renal oxygenation. On the basis of normal kidney physiology, the medulla sustains a state of hypoxia due to increased oxygen consumption for transcellular transport and sparser vascularization [72]. Decreased medullary R2* values at baseline were observed in allografts with acute rejection or acute tubular injury (ATI), compared with functioning grafts [73, 74]. Allografts with ATI showed significantly higher cortical and medullary R2* values compared with grafts with acute rejection [73, 74]. Measurements of the ratio of medullary-to-cortical R2* (MCR2*) in ATI and acute rejection compared with normally functioning grafts have shown conflicting results depending on the time interval between MRI and surgery (higher MCR2* in ATI than in normal allografts at 10 days after transplant [75] vs decreased MCR2* in ATI and acute rejection at a minimum of 29 days after transplant [73]). This difference can be explained by the fact that ischemia in early-stage ATI compromises oxygenation [72].

Arterial Spin Labeling

ASL uses magnetization of arterial water protons upstream of the tissue of interest as a freely diffusible endogenous tracer (Fig. 6). Renal plasma flow (RPF) measured by ASL is significantly, although modestly, correlated to RPF measured by reference standard methods [76]. In previous studies, cortical RPF values measured by ASL were statistically different between patients with stable allograft function and those with allograft dysfunction [77, 78] and correlated with eGFR [77]. Because allograft fibrosis is associated with capillary loss and impaired microvascular perfusion, reductions in ASL-derived blood flow may serve as a surrogate marker. In a prospective study of 175 patients, ASL renal blood flow (RBF) outperformed cortical ADC for distinction of renal allograft fibrosis and long-term allograft

dysfunction [79]. Endogenous contrast makes ASL useful for evaluation of patients with a transplant who cannot receive gadolinium-based contrast agents due to NSF risk. However, ASL has limitations compared with DCE-MRI [78], such as lower SNR [80], dependence on slice orientation with respect to main blood flow [81], and dependence on water proton exchange between capillaries and tissues [82]. ASL has great potential for clinical adoption because it is gadolinium-free and because the major MRI vendors have provided clinical and research ASL sequences.

Phase-Contrast MRI

PC-MRI measures velocity of moving protons using bipolar velocity-encoding magnetic field gradients to generate phase shifts proportional to protons' velocity in the gradient's direction. Flow measurements are most accurate when the imaging plane is perpendicular (through-plane) to the vessel of interest. PC-MRI data are typically collected in a breath-hold with retrospective or prospective cardiac gating to synchronize data acquisition with the cardiac cycle. Four-dimensional flow PC-MRI (Fig. 7) uses velocity encoding in three directions. This approach removes the need for detailed anatomic or vascular preparatory acquisitions for planning and allows simultaneous assessment of several vessels [51, 83]. A technical challenge of 2D or 4D PC-MRI is the choice of velocity encoding value (VENC), as underestimation of this parameter leads to velocity aliasing, whereas overestimation leads to inaccurate measurements. Ideally, the VENC should be as high as the renal arteries' typically observed peak velocities. For imaging allografts, choice of VENC is particularly challenging, because peak velocities can vary substantially among patients owing to tortuous circulation and different locations of the renal artery anastomosis. Motoyama et al. [83] addressed this problem by prescribing a 4D flow acquisition with patient-specific VENC, which was estimated on the basis of preparatory 2D PC-MRI measurements of renal artery peak velocity. Their study obtained equivalent image quality for the depiction of interlobar and arcuate renal arteries with 4D flow MRI as with CTA [83].

For PC-MRI analysis, an ROI is placed on the vessel of interest. To obtain arterial flux (in millimeters per minute) at each cardiac phase, the velocity (in centimeters per second) is multiplied by the area (in millimeters squared) in each frame. Global renal perfusion (in millimeters per minute per 100 mL of tissue) is calculated from the ratio of mean arterial flux by total kidney volume (in millimeters) multiplied by 100.

Although studies have used PC-MRI alone or in combination with other MRI sequences for diagnosis and characterization of CKD in native kidneys [84], PC-MRI has few applications in renal allografts. In an early study, RBF measured by PC-MRI in patients with functional renal transplants was highly concordant with reference standard RBF measurements by para-aminohippuric acid [85]. Another study examined one failed renal allograft by multiparametric MRI, including PC-MRI before nephrectomy; PC-MRI renal artery flow was 69% of normative values in healthy volunteers, a finding consistent with obliteration of interlobular arteries on histopathology [86]. A preliminary study with 4D flow MRI showed that flow in the renal artery and vein is reduced in patients with parenchymal allograft dysfunction with fibrosis and no renal artery stenosis, compared with patients with functional allografts [51].

The technical challenges involved in planning PC-MRI acquisitions (e.g., optimal choice of VENC and perpendicular location to the renal artery), lengthy acquisition times (e.g., 3–10 minutes for 4D flow MRI), and unavailability of commercial software packages for 4D flow MRI analysis have hampered widespread adoption of PC-MRI in kidney imaging. Future work may focus on calibration of 4D flow MRI using flow phantoms and validation of 2D PC-MRI and 4D flow MRI in patients with renal transplants in large multicenter studies.

MR Elastography

MR elastography (MRE) enables quantitative measurement of tissue stiffness by imaging propagation of mechanical shear waves through tissue. In MRE, tissue stiffness is measured as the magnitude of the complex shear modulus, derived from PC imaging of the wave propagation. Although MRE is well established for assessing liver fibrosis, MRE has shown confounding results for kidney assessment. Animal studies showed MRE measurements are influenced by blood flow [87], urinary flow [88], and tissue anisotropy, confounders that may mask the presence of fibrosis. Initial studies showed elevated stiffness in dysfunctional allografts [89–91] (as expected on the basis of elastography in liver fibrosis), but other studies showed decreased stiffness [92] or no difference in stiffness between dysfunctional and functional allografts [93]. Kennedy et al. [94] reported that mean and median allograft stiffness from MRE did not differentiate functional from dysfunctional allografts and did not correlate with Banff scores, although MRE of allograft stiffness predicted graft loss at 18 months after imaging. Another study with MRE in 55 patients with allograft biopsy found no correlation between allograft stiffness and Banff interstitial or glomerular fibrosis scores or quantitative assessment of fibrosis from histopathology [95]. In addition to the conflicting results from animal and human studies, the need for external hardware and specialized software to perform MRE further limits clinical adoption for renal transplant evaluation.

Fibrosis Quantification by Magnetization Transfer Imaging

A major shortcoming of MRI techniques such as DWI, T1 mapping, and MRE is that they cannot clearly differentiate renal allograft fibrosis from inflammation (DWI, T1) or hypoperfusion effects (MRE). Magnetization transfer imaging (MTI) is based on magnetization transfer between free water protons and protons bound to macromolecules. Saturation of macromolecules with off-resonance pulses induces a decrease in MR signal of free water protons, allowing a detectable change in MR signal, which is measured as the magnetization transfer ratio (MTR) of signal before and after application of off-resonance pulses. MTI is as sensitive to macromolecule content as T1 ρ mapping, but MTI is less dependent on tissue hemodynamics. These characteristics support MTI as a promising method to assess for renal allograft fibrosis. Also, unlike T1 ρ mapping, which requires specialized pulse sequences for acquisition, MTI protocols can be implemented from product sequences. In animals, MTR has been correlated with fibrosis at histopathology [96] and polycystic kidney disease cyst burden [97] and has been shown to be independent of renal ischemia [98]. However, an additional study showed correlation of MTR with RBF and glomerular filtration rate in a porcine model of renal artery stenosis after revascularization therapy [99]. In patients with CKD, MTR has shown correlation with eGFR [100].

Conclusion

MRI is the most clinically used imaging modality to assess for TRAS. Both enhanced (gadolinium and ferumoxytol) and unenhanced sequences are available. Advantages of ferumoxytol include long half-life and resulting higher resolution, which can be useful for assessing small graft renal arteries. However, the use of ferumoxytol as a contrast agent is off-label, and gadolinium-based agents are usually more readily available. Unenhanced MRA provides a useful alternative to contrast-enhanced MRA, particularly in patients with challenging IV access.

Novel MRI sequences have shown promise in parenchymal assessment of acute and chronic allograft kidney dysfunction. However, clear diagnostic thresholds for histopathologic diagnosis of allograft dysfunction have not emerged for individual parameters. Studies with larger sample sizes are needed to validate and compare these parameters' diagnostic performance.

References

1. Hariharan S, Israni AK, Danovitch G. Long-term survival after kidney transplantation. *N Engl J Med* 2021; 385:729–743 [PubMed: 34407344]
2. Nankivell BJ, Borrows RJ, Fung CL, O'Connell PJ, Allen RD, Chapman JR. The natural history of chronic allograft nephropathy. *N Engl J Med* 2003; 349:2326–2333 [PubMed: 14668458]
3. Nicholson ML, McCulloch TA, Harper SJ, et al. Early measurement of interstitial fibrosis predicts long-term renal function and graft survival in renal transplantation. *Br J Surg* 1996; 83:1082–1085 [PubMed: 8869307]
4. Sugi MD, Joshi G, Maddu KK, Dahiya N, Menias CO. Imaging of renal transplant complications throughout the life of the allograft: comprehensive multimodality review. *RadioGraphics* 2019; 39:1327–1355 [PubMed: 31498742]
5. Hurst FP, Abbott KC, Neff RT, et al. Incidence, predictors and outcomes of transplant renal artery stenosis after kidney transplantation: analysis of USRDS. *Am J Nephrol* 2009; 30:459–467 [PubMed: 19776559]
6. Fananapazir G, LaRoy JR, Navarro SM, Corwin MT, Carney B, Troppmann C. Ultrasound screening for transplant renal artery stenosis risk stratification using standardized criteria in structured reporting: a validation study. *J Ultrasound Med* 2022; 41:1433–1438 [PubMed: 34536039]
7. Fananapazir G, McGahan JP, Corwin MT, et al. Screening for transplant renal artery stenosis: ultrasound-based stenosis probability stratification. *AJR* 2017; 209:1064–1073 [PubMed: 28858538]
8. Huang Y, Zhang B, Zheng J, Ma X, Zhang S, Chen Q. Diagnostic performance of magnetic resonance angiography for artery stenosis after kidney transplant: a systematic review and meta-analysis. *Acad Radiol* 2023 Apr 17 [published online]
9. Boor P, Floege J. Renal allograft fibrosis: biology and therapeutic targets. *Am J Transplant* 2015; 15:863–886 [PubMed: 25691290]
10. Naesens M, Kuypers DR, De Vusser K, et al. The histology of kidney transplant failure: a long-term follow-up study. *Transplantation* 2014; 98:427–435 [PubMed: 25243513]
11. Naesens M, Kuypers DR, De Vusser K, et al. Chronic histological damage in early indication biopsies is an independent risk factor for late renal allograft failure. *Am J Transplant* 2013; 13:86–99
12. Menon MC, Keung KL, Murphy B, O'Connell PJ. The use of genomics and pathway analysis in our understanding and prediction of clinical renal transplant injury. *Transplantation* 2016; 100:1405–1414 [PubMed: 26447506]

13. Ho QY, Lim CC, Tan HZ, Sultana R, Kee T, Htay H. Complications of percutaneous kidney allograft biopsy: systematic review and meta-analysis. *Transplantation* 2022; 106:1497–1506 [PubMed: 35019898]
14. Bane O, Mendichovszky IA, Milani B, et al. Consensus-based technical recommendations for clinical translation of renal BOLD MRI. *Magn Reson Mater Biol Phys Med* 2020; 33:199–215
15. de Boer A, Villa G, Bane O, et al. Consensus-based technical recommendations for clinical translation of renal phase contrast MRI. *J Magn Reson Imaging* 2022; 55:323–335 [PubMed: 33140551]
16. Dekkers IA, de Boer A, Sharma K, et al. Consensus-based technical recommendations for clinical translation of renal T1 and T2 mapping MRI. *Magn Reson Mater Biol Phys Med* 2020; 33:163–176
17. Ljimini A, Caroli A, Laustsen C, et al. Consensus-based technical recommendations for clinical translation of renal diffusion-weighted MRI. *Magn Reson Mater Biol Phys Med* 2020; 33:177–195
18. Mendichovszky I, Pullens P, Dekkers I, et al. Technical recommendations for clinical translation of renal MRI: a consensus project of the Cooperation in Science and Technology Action PARENCHIMA. *Magn Reson Mater Biol Phys Med* 2020; 33:131–140
19. Nery F, Buchanan CE, Hartevelde AA, et al. Consensus-based technical recommendations for clinical translation of renal ASL MRI. *Magn Reson Mater Biol Phys Med* 2020; 33:141–161
20. Hohenwarter MD, Skowlund CJ, Erickson SJ, et al. Renal transplant evaluation with MR angiography and MR imaging. *RadioGraphics* 2001; 21:1505–1517 [PubMed: 11706221]
21. Law YM, Tay KH, Gan YU, Cheah FK, Tan BS. Gadolinium-enhanced magnetic resonance angiography in renal artery stenosis: comparison with digital subtraction angiography. *Hong Kong Med J* 2008; 14:136–141 [PubMed: 18382021]
22. Ismaeel MM, Abdel-Hamid A. Role of high resolution contrast-enhanced magnetic resonance angiography (HR CeMRA) in management of arterial complications of the renal transplant. *Eur J Radiol* 2011; 79:e122–e127 [PubMed: 21601400]
23. Vosschenrich R, Reimer P. Nephrogenic systemic fibrosis. *Vasa* 2009; 38:31–38 [PubMed: 19229801]
24. Gulani V, Calamante F, Shellock FG, Kanal E, Reeder SB; International Society for Magnetic Resonance in Medicine. Gadolinium deposition in the brain: summary of evidence and recommendations. *Lancet Neurol* 2017; 16:564–570 [PubMed: 28653648]
25. Schieda N, Krishna S, Davenport MS. Update on gadolinium-based contrast agent-enhanced imaging in the genitourinary system. *AJR* 2019; 212:1223–1233 [PubMed: 30973785]
26. Chan YL, Leung CB, Yu SC, Yeung DK, Li PK. Comparison of non-breath-hold high resolution gadolinium-enhanced MRA with digital subtraction angiography in the evaluation on allograft renal artery stenosis. *Clin Radiol* 2001; 56:127–132 [PubMed: 11222071]
27. Gaddikeri S, Mitsumori L, Vaidya S, Hippe DS, Bhargava P, Dighe MK. Comparing the diagnostic accuracy of contrast-enhanced computed tomographic angiography and gadolinium-enhanced magnetic resonance angiography for the assessment of hemodynamically significant transplant renal artery stenosis. *Curr Probl Diagn Radiol* 2014; 43:162–168 [PubMed: 24948209]
28. Hope MD, Hope TA, Zhu C, et al. Vascular imaging with ferumoxytol as a contrast agent. *AJR* 2015; 205:[web]W366–W373 [PubMed: 26102308]
29. Corwin MT, Fananapazir G, Chaudhari AJ. MR angiography of renal transplant vasculature with ferumoxytol: comparison of high-resolution steady-state and first-pass acquisitions. *Acad Radiol* 2016; 23:368–373 [PubMed: 26707344]
30. Gondalia R, Vernuccio F, Marin D, Bashir MR. The role of MR imaging in the assessment of renal allograft vasculature. *Abdom Radiol (NY)* 2018; 43:2589–2596 [PubMed: 29700591]
31. Fananapazir G, Bashir MR, Corwin MT, Lamba R, Vu CT, Troppmann C. Comparison of ferumoxytol-enhanced MRA with conventional angiography for assessment of severity of transplant renal artery stenosis. *J Magn Reson Imaging* 2017; 45:779–785 [PubMed: 27504713]
32. Zamecnik P, Israel B, Feuerstein J, et al. Ferumoxtran-10-enhanced 3-T magnetic resonance angiography of pelvic arteries: initial experience. *Eur Urol Focus* 2022; 8:1802–1808 [PubMed: 35337778]

33. Katoh M, Buecker A, Stuber M, Günther RW, Spuentrup E. Free-breathing renal MR angiography with steady-state free-precession (SSFP) and slab-selective spin inversion: initial results. *Kidney Int* 2004; 66:1272–1278 [PubMed: 15327427]
34. Wyttenbach R, Braghetti A, Wyss M, et al. Renal artery assessment with nonenhanced steady-state free precession versus contrast-enhanced MR angiography. *Radiology* 2007; 245:186–195 [PubMed: 17717326]
35. Mohrs OK, Petersen SE, Schulze T, et al. High-resolution 3D unenhanced ECG-gated respiratory-navigated MR angiography of the renal arteries: comparison with contrast-enhanced MR angiography. *AJR* 2010; 195:1423–1428 [PubMed: 21098205]
36. Lanzman RS, Voiculescu A, Walther C, et al. ECG-gated nonenhanced 3D steady-state free precession MR angiography in assessment of transplant renal arteries: comparison with DSA. *Radiology* 2009; 252:914–921 [PubMed: 19635833]
37. Zhang LJ, Peng J, Wen J, et al. Non-contrast-enhanced magnetic resonance angiography: a reliable clinical tool for evaluating transplant renal artery stenosis. *Eur Radiol* 2018; 28:4195–4204 [PubMed: 29666993]
38. Liu X, Berg N, Sheehan J, et al. Renal transplant: nonenhanced renal MR angiography with magnetization-prepared steady-state free precession. *Radiology* 2009; 251:535–542 [PubMed: 19261926]
39. Tang H, Wang Z, Wang L, et al. Depiction of transplant renal vascular anatomy and complications: unenhanced MR angiography by using spatial labeling with multiple inversion pulses. *Radiology* 2014; 271:879–887 [PubMed: 24592960]
40. Scheffler K, Lehnhardt S. Principles and applications of balanced SSFP techniques. *Eur Radiol* 2003; 13:2409–2418 [PubMed: 12928954]
41. Serhal A, Aouad P, Serhal M, et al. Evaluation of renal allograft vasculature using non-contrast 3D inversion recovery balanced steady-state free precession MRA and 2D quiescent-interval slice-selective MRA. *Explor Res Hypothesis Med* 2021; 6:90–98 [PubMed: 34589655]
42. Le Bihan D. Molecular diffusion nuclear magnetic resonance imaging. *Magn Reson Q* 1991; 7:1–30 [PubMed: 2043461]
43. Togao O, Doi S, Kuro-o M, Masaki T, Yorioka N, Takahashi M. Assessment of renal fibrosis with diffusion-weighted MR imaging: study with murine model of unilateral ureteral obstruction. *Radiology* 2010; 255:772–780 [PubMed: 20406881]
44. Hueper K, Rong S, Gutberlet M, et al. T2 relaxation time and apparent diffusion coefficient for noninvasive assessment of renal pathology after acute kidney injury in mice: comparison with histopathology. *Invest Radiol* 2013; 48:834–842 [PubMed: 23907103]
45. Hueper K, Khalifa AA, Bräsen JH, et al. Diffusion-weighted imaging and diffusion tensor imaging detect delayed graft function and correlate with allograft fibrosis in patients early after kidney transplantation. *J Magn Reson Imaging* 2016; 44:112–121 [PubMed: 26778459]
46. Friedli I, Crowe LA, Berchtold L, et al. New magnetic resonance imaging index for renal fibrosis assessment: a comparison between diffusion-weighted imaging and T1 mapping with histological validation. *Sci Rep* 2016; 6:30088 [PubMed: 27439482]
47. Beck-Tölly A, Eder M, Beitzke D, et al. Magnetic resonance imaging for evaluation of interstitial fibrosis in kidney allografts. *Transplant Direct* 2020; 15:e577
48. Wang W, Yu Y, Wen J, et al. Combination of functional magnetic resonance imaging and histopathologic analysis to evaluate interstitial fibrosis in kidney allografts. *Clin J Am Soc Nephrol* 2019; 14:1372–1380 [PubMed: 31416890]
49. Berchtold L, Friedli I, Crowe LA, et al. Validation of the corticomedullary difference in magnetic resonance imaging-derived apparent diffusion coefficient for kidney fibrosis detection: a cross-sectional study. *Nephrol Dial Transplant* 2020; 35:937–945 [PubMed: 30608554]
50. Hueper K, Gutberlet M, Bräsen JH, et al. Multiparametric functional MRI: non-invasive imaging of inflammation and edema formation after kidney transplantation in mice. *PLoS One* 2016; 11:e0162705 [PubMed: 27632553]
51. Bane O, Said D, Weiss A, et al. 4D Flow MRI for the assessment of renal transplant dysfunction: initial results. *Eur Radiol* 2021; 31:909–919 [PubMed: 32870395]

52. Le Bihan D, Breton E, Lallemand D, Aubin ML, Vignaud J, Laval-Jeantet M. Separation of diffusion and perfusion in intravoxel incoherent motion MR imaging. *Radiology* 1988; 168:497–505 [PubMed: 3393671]
53. Poynton CB, Lee MM, Li Y, et al. Intravoxel incoherent motion analysis of renal allograft diffusion with clinical and histopathological correlation in pediatric kidney transplant patients: a preliminary cross-sectional observational study. *Pediatr Transplant* 2017; 21:e12996
54. Eisenberger U, Thoeny HC, Binsler T, et al. Evaluation of renal allograft function early after transplantation with diffusion-weighted MR imaging. *Eur Radiol* 2010; 20:1374–1383 [PubMed: 20013274]
55. Bane O, Hectors SJ, Gordic S, et al. Multiparametric magnetic resonance imaging shows promising results to assess renal transplant dysfunction with fibrosis. *Kidney Int* 2020; 97:414–420 [PubMed: 31874802]
56. Fan M, Xing Z, Du Y, Pan L, Sun Y, He X. Quantitative assessment of renal allograft pathologic changes: comparisons of mono-exponential and bi-exponential models using diffusion-weighted imaging. *Quant Imaging Med Surg* 2020; 10:1286–1297 [PubMed: 32550137]
57. Hueper K, Gutberlet M, Rodt T, et al. Diffusion tensor imaging and tractography for assessment of renal allograft dysfunction: initial results. *Eur Radiol* 2011; 21:2427–2433 [PubMed: 21710264]
58. Gaudiano C, Clementi V, Busato F, et al. Diffusion tensor imaging and tractography of the kidneys: assessment of chronic parenchymal diseases. *Eur Radiol* 2013; 23:1678–1685 [PubMed: 23300038]
59. Lanzman RS, Ljimini A, Pentang G, et al. Kidney transplant: functional assessment with diffusion-tensor MR imaging at 3T. *Radiology* 2013; 266:218–225 [PubMed: 23169797]
60. Fan WJ, Ren T, Li Q, et al. Assessment of renal allograft function early after transplantation with isotropic resolution diffusion tensor imaging. *Eur Radiol* 2016; 26:567–575 [PubMed: 26017738]
61. Das CJ, Kubihal V, Kumar S, Agarwal SK, Dinda AK, Sreenivas V. Assessment of renal allograft rejection with diffusion tensor imaging. *Br J Radiol* 2023; 96:20220722 [PubMed: 36607279]
62. Malyarenko DI, Newitt D, Wilmes JL, et al. Demonstration of nonlinearity bias in the measurement of the apparent diffusion coefficient in multicenter trials. *Magn Reson Med* 2016; 75:1312–1323 [PubMed: 25940607]
63. Hueper K, Peperhove M, Rong S, et al. T1-mapping for assessment of ischemia-induced acute kidney injury and prediction of chronic kidney disease in mice. *Eur Radiol* 2014; 24:2252–2260 [PubMed: 24996794]
64. Aslam I, Aamir F, Kassai M, et al. Validation of automatically measured T1 map cortico-medullary difference ($T1$) for eGFR and fibrosis assessment in allograft kidneys. *PLoS One* 2023; 18:e0277277 [PubMed: 36791140]
65. Allkemper T, Sagmeister F, Cicinnati V, et al. Evaluation of fibrotic liver disease with whole-liver T1 ρ MR imaging: a feasibility study at 1.5 T. *Radiology* 2014; 271:408–415 [PubMed: 24475807]
66. Wang YX, Yuan J, Chu ES, et al. T1rho MR imaging is sensitive to evaluate liver fibrosis: an experimental study in a rat biliary duct ligation model. *Radiology* 2011; 259:712–719 [PubMed: 21436087]
67. van Oorschot JW, Güçlü F, de Jong S, et al. Endogenous assessment of diffuse myocardial fibrosis in patients with T1 ρ -mapping. *J Magn Reson Imaging* 2017; 45:132–138 [PubMed: 27309545]
68. Rapacchi S, Smith RX, Wang Y, et al. Towards the identification of multi-parametric quantitative MRI biomarkers in lupus nephritis. *Magn Reson Imaging* 2015; 33:1066–1074 [PubMed: 26119419]
69. Hectors SJ, Bane O, Kennedy P, et al. T1 ρ mapping for assessment of renal allograft fibrosis. *J Magn Reson Imaging* 2019; 50:1085–1091 [PubMed: 30666744]
70. Menezes NM, Gray ML, Hartke JR, Burstein D. T2 and T1rho MRI in articular cartilage systems. *Magn Reson Med* 2004; 51:503–509 [PubMed: 15004791]
71. Zhao F, Wang YX, Yuan J, et al. MR T1 ρ as an imaging biomarker for monitoring liver injury progression and regression: an experimental study in rats with carbon tetrachloride intoxication. *Eur Radiol* 2012; 22:1709–1716 [PubMed: 22752522]
72. Zhang JL, Rusinek H, Chandarana H, Lee VS. Functional MRI of the kidneys. *J Magn Reson Imaging* 2013; 37:282–293 [PubMed: 23355431]

73. Djamali A, Sadowski EA, Samaniego-Picota M, et al. Noninvasive assessment of early kidney allograft dysfunction by blood oxygen level-dependent magnetic resonance imaging. *Transplantation* 2006; 82:621–628 [PubMed: 16969284]
74. Park SY, Kim CK, Park BK, Huh W, Kim SJ, Kim B. Evaluation of transplanted kidneys using blood oxygenation level-dependent MRI at 3 T: a preliminary study. *AJR* 2012; 198:1108–1114 [PubMed: 22528900]
75. Han F, Xiao W, Xu Y, et al. The significance of BOLD MRI in differentiation between renal transplant rejection and acute tubular necrosis. *Nephrol Dial Transplant* 2008; 23:2666–2672 [PubMed: 18308769]
76. Ritt M, Janka R, Schneider MP, et al. Measurement of kidney perfusion by magnetic resonance imaging: comparison of MRI with arterial spin labeling to para-aminohippuric acid plasma clearance in male subjects with metabolic syndrome. *Nephrol Dial Transplant* 2010; 25:1126–1133 [PubMed: 19934080]
77. Heusch P, Wittsack HJ, Blondin D, et al. Functional evaluation of transplanted kidneys using arterial spin labeling MRI. *J Magn Reson Imaging* 2014; 40:84–89 [PubMed: 24123319]
78. Lanzman RS, Wittsack HJ, Martirosian P, et al. Quantification of renal allograft perfusion using arterial spin labeling MRI: initial results. *Eur Radiol* 2010; 20:1485–1491 [PubMed: 19949799]
79. Yu YM, Wang W, Wen J, Zhang Y, Lu GM, Zhang LJ. Detection of renal allograft fibrosis with MRI: arterial spin labeling outperforms reduced field-of-view IVIM. *Eur Radiol* 2021; 31:6696–6707 [PubMed: 33738596]
80. Karger N, Biederer J, Lüsse S, et al. Quantitation of renal perfusion using arterial spin labeling with FAIR-UFLARE. *Magn Reson Imaging* 2000; 18:641–647 [PubMed: 10930773]
81. Lin YR, Wu MT, Huang TY, et al. Comparison of arterial spin labeling and first-pass dynamic contrast-enhanced MR imaging in the assessment of pulmonary perfusion in humans: the inflow spin-tracer saturation effect. *Magn Reson Med* 2004; 52:1291–1301 [PubMed: 15562497]
82. Warmuth C, Gunther M, Zimmer C. Quantification of blood flow in brain tumors: comparison of arterial spin labeling and dynamic susceptibility-weighted contrast-enhanced MR imaging. *Radiology* 2003; 228:523–532 [PubMed: 12819338]
83. Motoyama D, Ishii Y, Takehara Y, et al. Four-dimensional phase-contrast vastly undersampled isotropic projection reconstruction (4D PC-VIPR) MR evaluation of the renal arteries in transplant recipients: preliminary results. *J Magn Reson Imaging* 2017; 46:595–603 [PubMed: 28152259]
84. Villa G, Ringgaard S, Hermann I, et al. Phase-contrast magnetic resonance imaging to assess renal perfusion: a systematic review and statement paper. *Magn Reson Mater Biol Phys Med* 2020; 33:3–21
85. Myers BD, Sommer FG, Li K, et al. Determination of blood flow to the transplanted kidney: a novel application of phase-contrast, cine magnetic resonance imaging. *Transplantation* 1994; 57:1445–1450 [PubMed: 8197605]
86. de Boer A, Pieters TT, Hartevelde AA, et al. Validation of multiparametric MRI by histopathology after nephrectomy: a case study. *Magn Reson Mater Biol Phys Med* 2021; 34:377–387
87. Warner L, Yin M, Glaser KJ, et al. Noninvasive in vivo assessment of renal tissue elasticity during graded renal ischemia using MR elastography. *Invest Radiol* 2011; 46:509–514 [PubMed: 21467945]
88. Gennisson JL, Grenier N, Combe C, Tanter M. Supersonic shear wave elastography of in vivo pig kidney: influence of blood pressure, urinary pressure and tissue anisotropy. *Ultrasound Med Biol* 2012; 38:1559–1567 [PubMed: 22698515]
89. Ghonge NP, Mohan M, Kashyap V, Jasuja S. Renal allograft dysfunction: evaluation with shear-wave sonoelastography. *Radiology* 2018; 288:146–152 [PubMed: 29634441]
90. He WY, Jin YJ, Wang WP, Li CL, Ji ZB, Yang C. Tissue elasticity quantification by acoustic radiation force impulse for the assessment of renal allograft function. *Ultrasound Med Biol* 2014; 40:322–329 [PubMed: 24315391]
91. Kirpalani A, Hashim E, Leung G, et al. Magnetic resonance elastography to assess fibrosis in kidney allografts. *Clin J Am Soc Nephrol* 2017; 12:1671–1679 [PubMed: 28855238]

92. Marticorena Garcia SR, Fischer T, Dürr M, et al. Multifrequency magnetic resonance elastography for the assessment of renal allograft function. *Invest Radiol* 2016; 51:591–595 [PubMed: 27504796]
93. Lee J, Oh YT, Joo DJ, et al. Acoustic radiation force impulse measurement in renal transplantation: a prospective, longitudinal study with protocol biopsies. *Medicine (Baltimore)* 2015; 94:e1590 [PubMed: 26426636]
94. Kennedy P, Bane O, Hectors SJ, et al. Magnetic resonance elastography vs. point shear wave ultrasound elastography for the assessment of renal allograft dysfunction. *Eur J Radiol* 2020; 130:109180 [PubMed: 32736305]
95. Chauveau B, Merville P, Soulabaille B, et al. Magnetic resonance elastography as surrogate marker of interstitial fibrosis in kidney transplantation: a prospective study. *Kidney360* 2022; 3:1924–1933 [PubMed: 36514413]
96. Wang F, Wang S, Zhang Y, et al. Noninvasive quantitative magnetization transfer MRI reveals tubulointerstitial fibrosis in murine kidney. *NMR Biomed* 2019; 32:e4128 [PubMed: 31355979]
97. Kline TL, Irazabal MV, Ebrahimi B, et al. Utilizing magnetization transfer imaging to investigate tissue remodeling in a murine model of autosomal dominant polycystic kidney disease. *Magn Reson Med* 2016; 75:1466–1473 [PubMed: 25974140]
98. Jiang K, Ferguson CM, Woollard JR, et al. Magnetization transfer imaging is unaffected by decreases in renal perfusion in swine. *Invest Radiol* 2019; 54:681–688 [PubMed: 31261296]
99. Afarideh M, Jiang K, Ferguson CM, Woollard JR, Glockner JF, Lerman LO. Magnetization transfer imaging predicts porcine kidney recovery after revascularization of renal artery stenosis. *Invest Radiol* 2021; 56:86–93 [PubMed: 33405430]
100. Ito K, Hayashida M, Izumitani S, Fujimine T, Onishi T, Genba K. Magnetisation transfer MR imaging of the kidney: evaluation at 3.0 T in association with renal function. *Eur Radiol* 2013; 23:2315–2319 [PubMed: 23591620]

Highlights

- Confirmation of transplant renal artery stenosis by MRA, using gadolinium-enhanced, ferumoxytol-enhanced, or unenhanced techniques, may decrease invasive angiography for diagnostic purposes.
- Functional MRI sequences show promise in assessing acute and chronic kidney dysfunction.
- Functional MRI sequences are largely investigational and require validation studies.

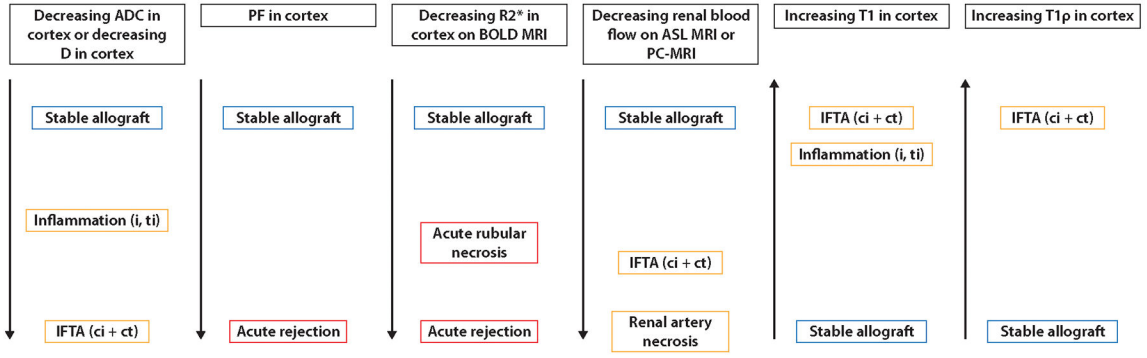


Fig. 1— Illustration shows changes (decreases or increases) in quantitative MRI metrics used for diagnosis of renal allograft parenchymal dysfunction based on published literature. From left to right, metrics are ADC on DWI, true intracellular water diffusion (D) on intravoxel incoherent motion DWI (IVIM-DWI), perfusion fraction (PF) on IVIM-DWI, transverse relaxation rate (R2*) on blood oxygenation level–dependent (BOLD) MRI, renal blood flow measured by arterial spin-labeling (ASL) or phase-contrast MRI (PC-MRI), T1, and T1ρ. Metrics are measured in renal cortex given that these metrics are typically correlated to invasive histopathologic classification from core needle biopsy, which samples primarily renal cortex. Blue boxes indicate stable (normally functioning) allograft, red boxes indicate acute allograft dysfunction (i.e., acute rejection or acute tubular necrosis), and yellow boxes indicate chronic allograft dysfunction (i.e., interstitial fibrosis or tubular atrophy [IFTA] measured by Banff score, which is composed of quantitative criteria for interstitial fibrosis [ci] + quantitative criteria for tubular atrophy [ct], renal artery stenosis, or interstitial inflammation [i] or tubular inflammation [ti]).

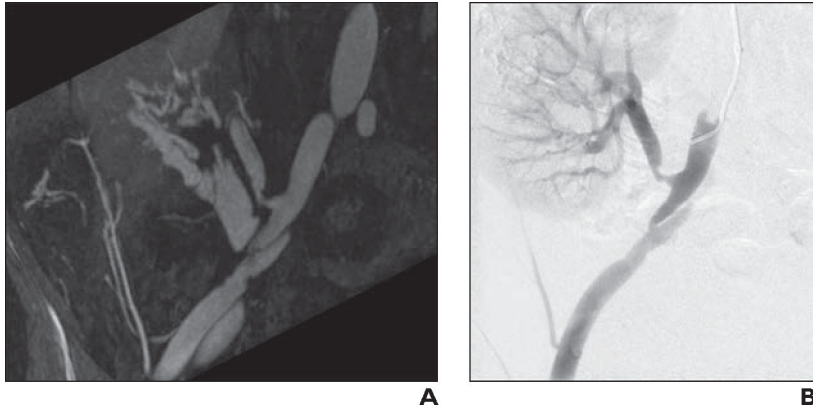


Fig. 2—
66-year-old man with renal transplant who presented for MRA and digital subtraction angiography (DSA) after ultrasound showed very high risk of transplant renal artery stenosis.
A, Ferumoxytol-enhanced MRA of transplant renal artery shows greater than 50% narrowing of proximal renal artery. Incidentally noted is dissection of more distal external iliac artery.
B, DSA confirms narrowing of proximal renal artery as well as external iliac artery dissection.

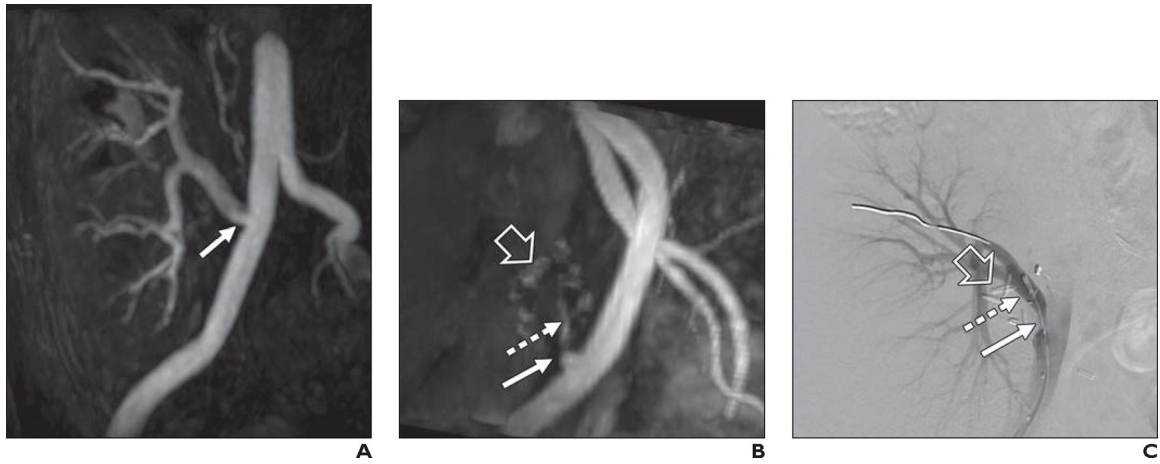
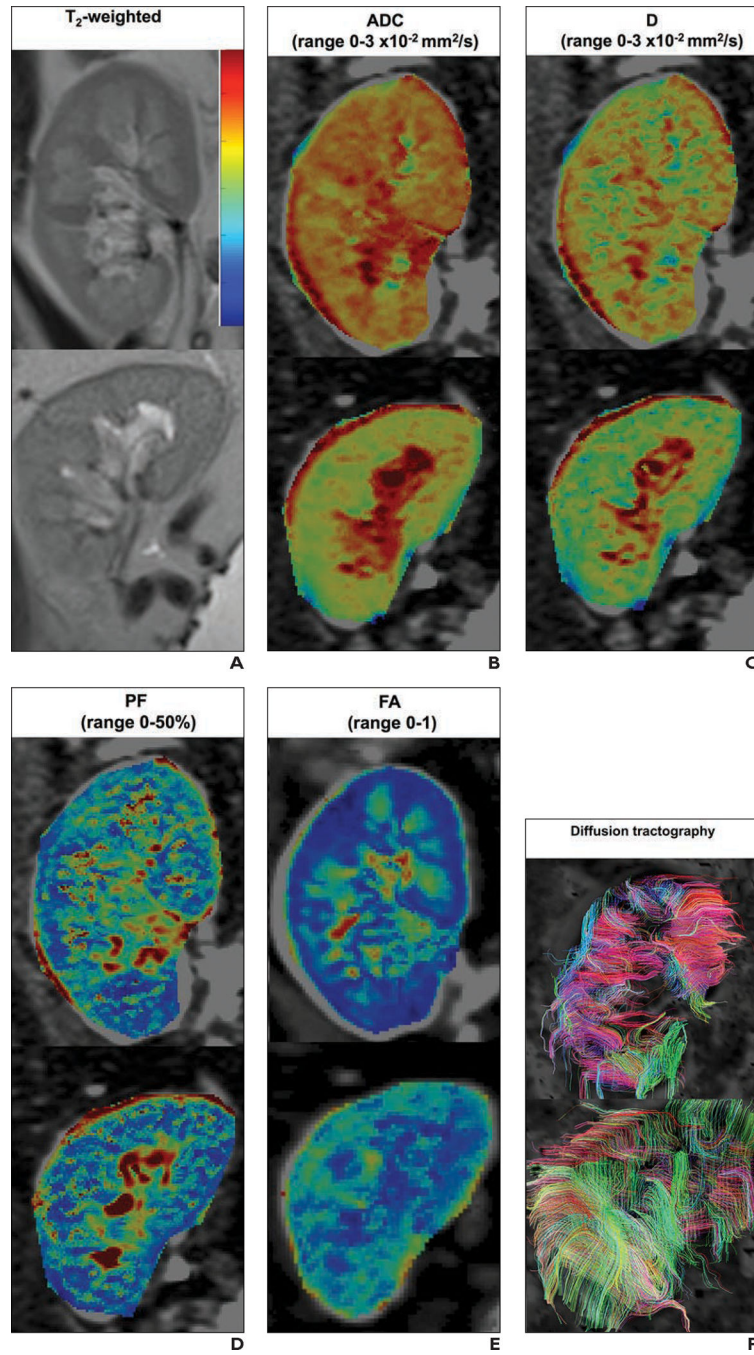


Fig. 3— MRA and digital subtraction angiography (DSA) images of patients who underwent renal transplant. (Courtesy of Hecht EM, Weill Cornell Medicine, New York, NY) **A**, 33-year-old woman who underwent renal transplant 2 years earlier. Unenhanced MRA using inflow inversion recovery (IFIR) shows mild ostial narrowing of transplant renal artery (*arrow*). Intrarenal arteries are well depicted with IFIR as background renal parenchymal signal is suppressed by selective radiofrequency pulse. **B** and **C**, 55-year-old patient with renal transplant and new hypertension. On unenhanced MRA (**B**), only ostium of transplant renal artery (*solid arrow, B*) is well seen, and more distal transplant artery (*dashed arrow, B*) is only intermittently visualized. Multiple surgical clips (*open arrow, B*) are present in operative bed. Poor visualization of distal artery is suspected to be due to combination of turbulent flow distal to severe transplant renal artery stenosis and poor suppression of background signal owing to susceptibility artifact. DSA (**C**) confirms severe proximal stenosis (*solid arrow, C*), which was subsequently stented. Although vessels beyond stenosis are poorly visualized, this case highlights high sensitivity of unenhanced MRA for hemodynamically significant stenosis such that unenhanced MRA is sufficient as screening test to suggest further evaluation with possible intervention. In **C**, dashed arrow also shows distal transplant artery, and open arrow shows surgical clip.



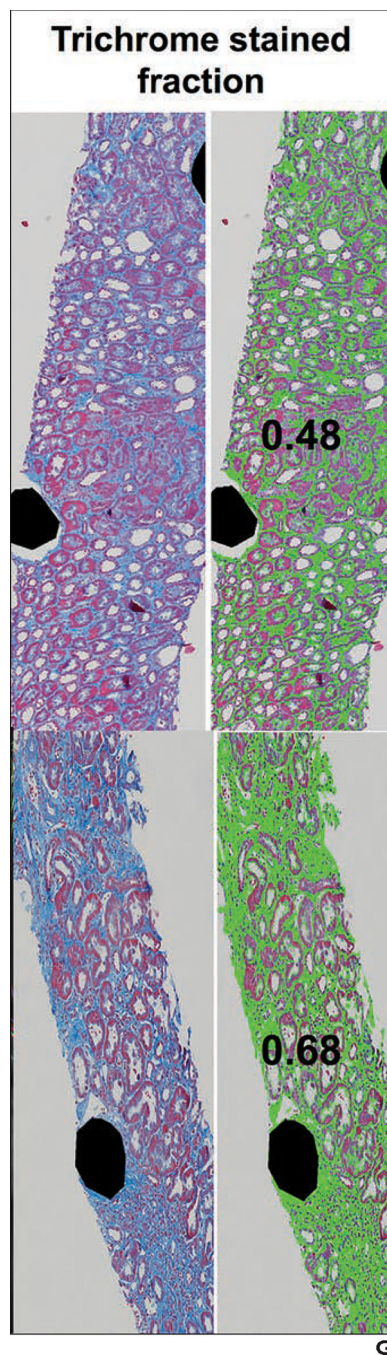


Fig. 4— 55-year-old woman with functional renal allograft (estimated glomerular filtration rate [eGFR] = 78.4 mL/min/1.73 m²) (*top images*) and 38-year-old woman with renal allograft fibrosis (eGFR = 19.9 mL/min/1.73 m²) (*bottom images*). In patient with renal allograft fibrosis, biopsy performed for acute kidney injury showed moderate interstitial fibrosis or tubular atrophy (Banff score: quantitative criteria for interstitial fibrosis [ci] + quantitative criteria for tubular atrophy [ct] = 2 + 2).

A–C, Representative T2-weighted images (**A**), ADC maps (**B**) (ADC range = $0\text{--}3 \times 10^{-2}$ mm²/s), and intravoxel incoherent motion parametric maps (**C**) (intracellular water diffusion [D] range = $0\text{--}3 \times 10^{-2}$ mm²/s).

D–F, Perfusion fraction (PF) images (**D**) (PF range = 0–50%), fractional anisotropy (FA) maps (**E**) (FA range = 0–1), and diffusion tractography volume renderings (**F**).

G, Photomicrographs (Masson trichrome stain, $\times 20$) from biopsy samples of functional renal transplant (*top images*) and renal allograft with fibrosis (*bottom images*). Collagen is stained blue in left images, and collagen quantification overlay is shown in green on right images (stained fraction of collagen = 0.48 for functional allograft and 0.68 for fibrotic allograft).

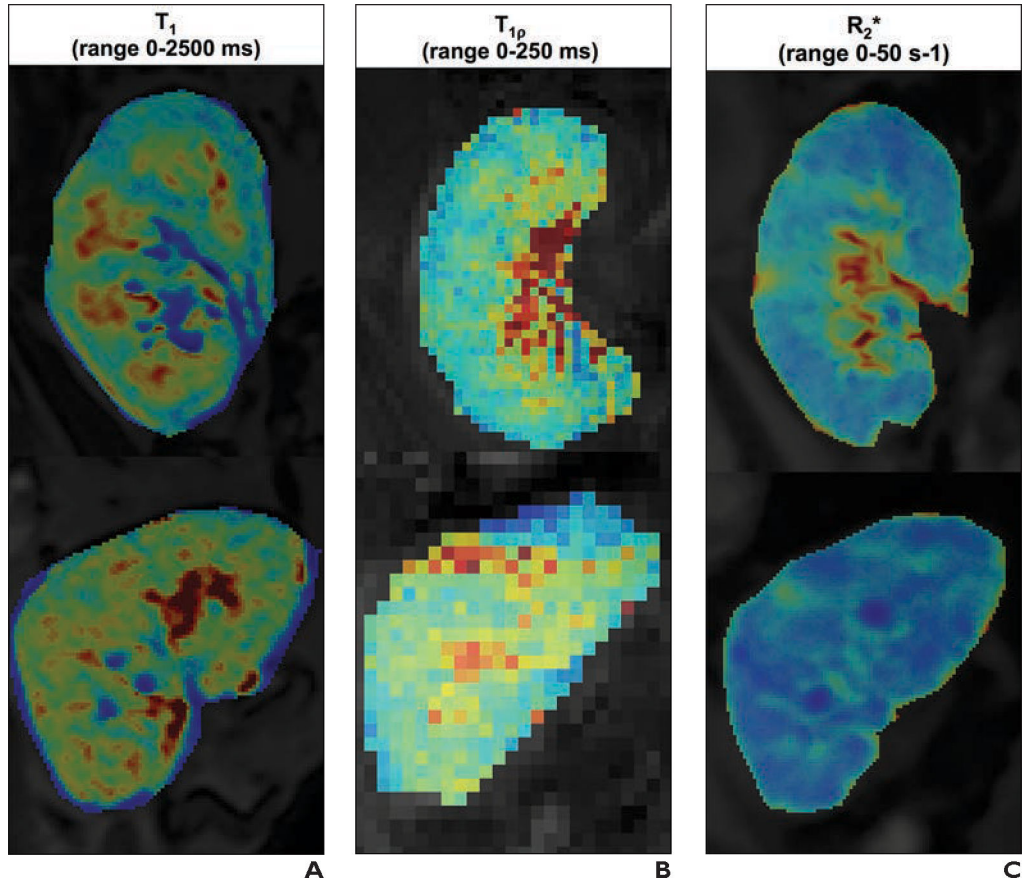


Fig. 5—.

55-year-old woman (same patient as in Fig. 4) with functional renal allograft (estimated glomerular filtration rate [eGFR] = 78.4 mL/min/1.73 m²) (*top images*) and 38-year-old woman (same patient as in Fig. 4) with renal allograft fibrosis (eGFR = 19.9 mL/min/1.73 m²) (*bottom images*). In patient with renal allograft fibrosis, biopsy performed for acute kidney injury showed moderate interstitial fibrosis or tubular atrophy (Banff score: quantitative criteria for interstitial fibrosis [ci] + quantitative criteria for tubular atrophy [ct] = 2 + 2).

A, T1 relaxometry maps show T1 (T1 range = 0–2500 ms).

B, T1ρ relaxometry maps show T1ρ (T1ρ range = 0–250 ms).

C, Transverse relaxation rate (R2*) relaxometry maps show R2* (R2* range = 0–50 s⁻¹).

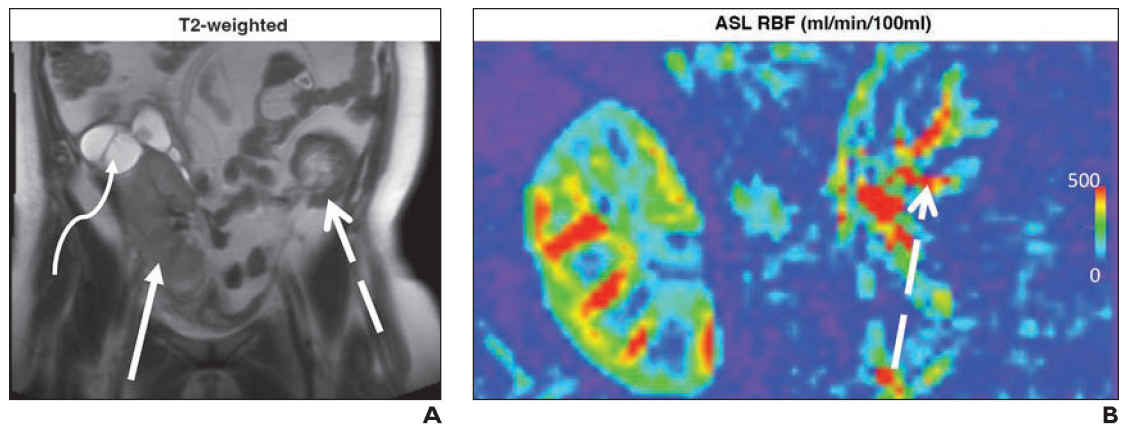


Fig. 6—
30-year-old woman with two failed renal allografts and one functional renal allograft.
A, T2-weighted MR image shows failed cystic right-sided allograft (*curved arrow*), failed left-sided fibrotic allograft (*dashed arrow*), and functional renal allograft (*solid straight arrow*).
B, Arterial spin-labeling renal blood flow map shows residual perfusion from left-sided failed renal allograft (*arrow*). Scale is in milliliters per minute per 100 mL of tissue.

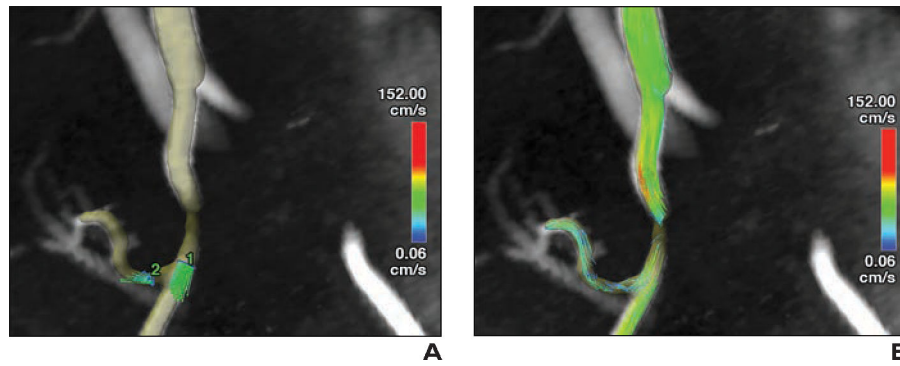


Fig. 7— 42-year-old man with right-sided renal allograft with severe fibrosis (inflammatory interstitial fibrosis or tubular atrophy score of 3; Banff score: quantitative criteria for interstitial fibrosis [ci] + quantitative criteria for tubular atrophy [ct] = 3 + 2). **A** and **B**, Four-dimensional flow phase-contrast MRA (**A**) and particle tracing image (**B**) show arterial inflow to allograft in ROI perpendicular to renal artery. Flow vectors and particle traces are near anastomosis to right iliac artery. In **A**, ROI 1 shows XXX and ROI 2 shows XXX.